Molecular and Electronic Structure of a Reduced Schiff Base Cryptand: Characterization by X-ray Crystallography and Optical and EPR/ENDOR Spectroscopy

Andrew S. Ichimura, Qingshan Xie, Lawrence P. Szajek, Julius Lema, Amy Burns, Rui H. Huang, James E. Jackson, and James L. Dye*

Department of Chemistry and Center for Fundamental Materials Research, Michigan State University, East Lansing, Michigan 48824

Franck Demol, Francois X. Sauvage, and Marc G. DeBacker*

LASIR-HEI, UMR 8516 CNRS, 13 rue de Toul, 59046 Lille Cedex, France

Received: November 22, 1999; In Final Form: January 27, 2000

The macrobicyclic Schiff base cryptand, **1**, with a *m*-phenyl group in each of the arms was reduced in tertrahydrofuran with the alkali metals Na through Cs to yield mono-, di-, and trianions. The crystal structure of a salt of $\mathbf{1}^-$, formed by reduction of **1** with potassium metal in mixed dimethyl ether−methylamine solutions, shows that K^+ is *not* encapsulated in the cavity of the cryptand. Instead, it forms methylamine-separated ion pairs arranged in symmetric fashion to give overall C_3 symmetry. Solution studies by optical and EPR/ENDOR spectroscopies revealed complex ion pair equilibria that are compatible with *external* contact ion pair and solvent-separated ion pair formation. The rate of electron (and cation) transfer between strands is $<4 \times 10^7$ s^{-1} for contact pairs, but faster for solvent-separated pairs. The addition of cryptand [2.2.2] to complex K^+ breaks up the contact ion pairs and yields behavior similar to that of solvent-separated ion pairs. Cyclic voltammetry revealed three partially reversible reduction waves. Both the dianion and trianion were formed in solution by reduction with potassium and studied by optical and EPR spectroscopies. Two compounds, **2** and **3**, which model a single strand of the macrobicycle, were used to deconvolute the spectra of $\mathbf{1}^-$. The monoanions, $\mathbf{2}^-$ and $\mathbf{3}^-$, are in equilibrium with a diamagnetic dimer that may be related to the pinacolate structure of the analogous ketyl dimers.

Introduction

The study of radical anions in solution, formed by the reduction of an organic electron acceptor and an alkali metal, is a mature field.[1,2] Characterization by optical and electron paramagnetic resonance (EPR) spectroscopies provides information on the equilibria between ion pairs, solvent-separated pairs, and free ions and on the molecular and electronic structures of such species in solution. Solvated electrons, on the other hand, can be formed by dissolving alkali metals in solvents such as ammonia and primary amines or in less polar solvents such as THF or dimethyl ether when crown ethers or cryptands are present. Characterizing the properties of such solutions has become a separate and well-developed field of study unto itself.[3,4] Interestingly, both radical anions and solvated electrons have their respective solid-state crystalline counterparts in the form of radical anion salts[5−13] and electrides.[14] Both systems are ionic but are as fundamentally different as the solutions from which crystals are grown. Electrides consist of complexed alkali metal cations and "trapped" electrons, while aromatic molecules form organic radical anion salts upon reduction with alkali metals. Electrides exhibit cooperative behavior such as one-dimensional antiferromagnetism and can range from insulators to semimetals,[14] but the solid-state properties of radical anion salts are less well-known.

The current work is part of a program to develop complexants that would bridge the gap between electrides and radical anion salts. Conceptually, the two extremes may be combined in a complexant that incorporates both the cation binding ability and *partial* reducibility. Encapsulating the cation within the cryptand with the negative charge distributed on the cryptand itself would form a neutral complex. Two recent examples of this type are sodio-cryptatium[15−17] and $[Ru(bipy)_3]^0$.[18−20] The former has a sodium cation trapped within a tri-bipyridyl cryptand and one electron localized on the complexant. The latter was prepared by electrochemical reduction and crystallization from $[Ru(bipy)_3]^{2+}$ and has two electrons on the organic substrate. Both crystalline compounds may be considered to have unpaired electron spin density distributed over the complexant molecules, although the latter has reasonable conductivity[19] and may have "excess" electron density in the void spaces as well.[20] On the other hand, alkali metal adducts to C_{60} have the cations in tetrahedral and octahedral vacancies created by packing of the large C_{60} moieties. The resulting salts display delocalized magnetic[21] and conductive[22] behavior that depends on the extent of reduction. The discovery of the superconductivity of M_3C_{60} at temperatures close to 40 K sparked a great deal of interest in these systems.[23] Our efforts are focused on *molecular* materials that can both complex alkali metal cations and accept electrons.

A large variety of complexant molecules remain to be explored. Possible candidates for both alkali cation encapsulation and reduction are hexa-imine macrobicyclic Schiff base cryptands with aromatic linking groups. We have synthesized a series of Schiff base cryptands with linking groups such as biphenyl, naphthalene, furan, and so forth. Alkali metals or electrochemical methods can be used to reduce the aromatic groups, and the imine nitrogen atoms with partial negative charge should

10.1021/jp994149c CCC: $19.00
Published on Web 03/11/2000

be able to bind metal cations. The ability to encapsulate alkali cations within the cryptand cavity was uncertain at the start of this work. This work describes the reduction chemistry of the *m*-phenyl-linked Schiff base cryptand **1**.

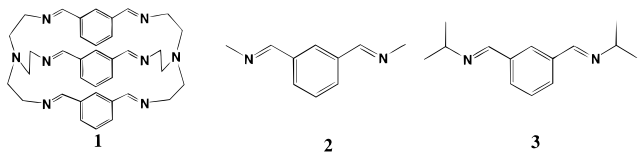

1 **2** **3**

Reduction of **1** by alkali metals in THF yielded, after solvent removal, radical anion salts that could not be isolated as crystals.[24] These solids were paramagnetic and their conductivity was semiconductor-like. They were stable at room temperature and the organic molecule was not modified in the process as shown by the observation of the NMR spectrum of **1** from a solid sample quenched with D_2O. (Note that we use $\mathbf{1}^-$, $\mathbf{1}^{2-}$, $\mathbf{2}^-$, and so forth to designate the anions, whether or not they are radical ions.)

We report here the crystal structure of the monoanion salt formed by reduction of **1** with potassium in mixed dimethyl ether−methylamine solutions, the solution phase electrochemistry, and the optical and EPR spectra for the mono-, di-, and trianions of **1**. The proton hyperfine splitting parameters of $\mathbf{1}^-$ were obtained by electron nuclear double-resonance spectroscopy (ENDOR). To help determine the "excess" electron distribution in $\mathbf{1}^-$, two model compounds, **2** and **3**, that are essentially one strand of **1** were reduced and studied in dilute THF solutions by optical, EPR, and ENDOR spectroscopies as well as by cyclic voltammetry (CV).

Experimental Section

General. The synthesis of the macrobicyclic Schiff base cryptands and that of the model compounds followed procedures described in the literature.[25,26] All reagents and solvents were purified by vacuum distillation before use. All handling and weighings were performed in an oxygen-free, helium-filled glovebox.

Crystal Growth. Measured quantities of the Schiff base cryptand and potassium metal were placed in separate sides of a K-cell.[27] After evacuation to $\sim 10^{-5}$ Torr, a metal mirror was formed. Dimethyl ether (~15 mL) was distilled into the K-cell at 210 K and the cryptand was dissolved. The resulting solution was poured over the metal mirror and ~2 mL of methylamine was added. Rapid reaction of the metal and cryptand formed a dark green-colored solution. At −78 °C, ~5 mL of diethyl ether was added as a cosolvent to saturate the solution until some dark solids appeared. The saturated solution was poured through a frit back to the first chamber. Crystals were grown by slow evaporation of the dimethyl ether at 200 K. The crystals decompose in the presence of oxygen or water and even under vacuum at ambient temperatures (probably due to the removal of methylamine).

Optical and EPR/ENDOR Spectra. A quartz optical cell and a Suprasil quartz EPR tube were attached to a K-cell so that EPR and optical spectra could be obtained from the same initial sample. Stoichiometric amounts of the alkali metal and the Schiff base cryptand were used to form the desired mono-, di-, or trianion. Completion of the reduction was indicated by the disappearance of the alkali metal film. This occurred rapidly for preparation of the mono- and dianions but required 2−3 days with occasional agitation to complete the formation of the trianion. The solutions were kept below ~230 K to ensure stability. Samples for optical, EPR, and ENDOR spectroscopy had concentrations between 0.5 and 3 mM.

Optical spectra in the visible and near-infrared (NIR) region were obtained with a Guided Wave model 250 spectrometer utilizing a cell with a 1.0-mm path length. In some cases, temporary dilution of the solution in the cell was necessary to keep the spectra on scale. As a result, only specral shapes and not extinction coefficients were obtained. A home-built N_2 gas flow-through system permitted temperature control during acquisition of the spectra. A Bruker (9.5 GHz) ESP-300E electron spin resonance spectrometer equipped with a DICE ENDOR unit was used to acquire EPR and ENDOR spectra. Temperature was controlled with an Oxford Instruments 9000 liquid helium cryostat. The *g*-values were measured by determining the field and microwave frequency with a Bruker ER035M NMR gaussmeter and EIP model 25B frequency counter.

Electrochemistry. The supporting electrolyte, tetrabutylammonium hexafluorophosphate ($TBAPF_6$), was recrystallized twice from absolute ethanol and dried under vacuum at room temperature prior to use. Concentrations of ~1 mM in the Schiff base cryptand or single-strand molecules and 100 mM in $TBAPF_6$ were used. Measurements were made with a home-built three-electrode compartment vacuum cell. The working electrode was a glassy carbon electrode (BAS), the pseudo-reference was a fresh surface silver wire, and the counter electrode was a platinum wire. Cyclic voltammetry measurements were made on a EG&G Princeton Applied Research potentiostat/galvanostat model 273 and a BAS CV-50W voltammetric analyzer. A sweep rate of 0.1 V s^{-1} was used and a 100% IR compensation was achieved before each run. The final results were calibrated with the ferrocene/ferrocinium couple.

X-ray Crystallography. The procedure used to handle these reactive air-sensitive crystals was similar to that used with electrides.[27] Crystals were stored under vacuum at liquid nitrogen temperature until used. The black crystals were transferred in a nitrogen-filled glovebag to a depression in a cooled copper block (210 K) filled with purified octane. After examination with a microscope, a suitable crystal was picked up with a glass fiber that had vacuum grease on its tip and transferred to the precooled X-ray sample chamber while being kept in a stream of cold nitrogen gas. The crystal was maintained at 173 K during data collection with a Siemens P3 diffractometer equipped with a low-temperature accessory.

Results

Crystal Structure. The crystal structure is shown in Figure 1 and the structural parameters are listed in Table 1. A view down the 3-fold *c*-axis (Figure 1a) shows the high symmetry of the crystal. The Schiff base cryptand monoanion salt contains solvent-separated ion pairs in which the potassium cations are *outside* of the cryptand molecule and are coordinated to six methylamine molecules. The K^+−N distance (to the methylamine nitrogen) is 2.981 Å and the K^+−K^+ distance is 8.005 Å. The Schiff base nitrogens are too far from the nearest K^+, 5.294 Å, to participate in the coordination sphere, but may form hydrogen bonds to the closest methylamine nitrogens that are only 3.20 and 3.29 Å away. The anions and solvated cations form columns that alternate in the crystal. A second view nearly perpendicular to the *c*-axis is shown in Figure 1b. The Schiff base groups and the phenyl ring are nearly planar, although the Schiff base nitrogen atoms are about 8° out of the plane of the phenyl ring. A remarkable feature of $\mathbf{1}^-$ is its high *molecular* symmetry, C_3. All three strands of the cryptand are crystallo-

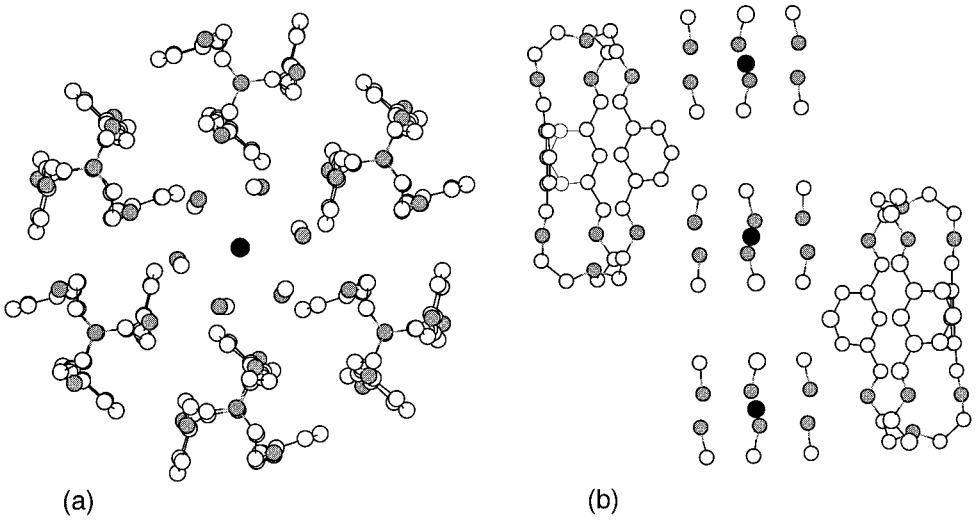

Figure 1. The crystal structure of $K^+\mathbf{1}^-(MeNH_2)_6$ shown (a) along the 3-fold *c*-axis and (b) perpendicular to the *c*-axis with several anions removed for clarity. Open, shaded, and black circles represent C, N, and K atoms, respectively.

TABLE 1: Crystallographic and Refinement Data for $K^+\mathbf{1}^-(MeNH_2)_6$

	$K^+\mathbf{1}^-(MeNH_2)_6$
space group	trigonal, $P\bar{3}$
crystal dimensions	0.4 × 0.5 × 0.5 mm
cell parameters	
a, Å	13.157(3)
b, Å	13.157(3)
c, Å	16.011(7)
α, deg	90.00
β, deg	90.00
γ, deg	120.00
z	6
scan type	*ω*
maximum 2*θ*	50°
temperature, K	173
no. of reflections collected	2544
no. of unique reflections	2272
no. of reflections used in refinement with $F_0^2 > 2\sigma(F_0^{2})$	1282
no. of variables	173
R	0.097
high peak in F-map	0.96 e/Å^3

graphically equivalent, in contrast to cryptatium, which has one strand that is distinctly different from the other two.[15] The high symmetry of the radical anion suggests that the unpaired electron is, on the average, delocalized over all three strands of the macrobicycle. One electron delocalized over three strands is not a large perturbation; hence, neutral[25] and reduced **1** are virtually identical in structure.

Optical Spectroscopy. In our system, the only species that contribute to the optical spectra at wavelengths greater than 300 nm are the anions or their reaction products. Solutions that have a 1:1 stoichiometric amount of the Schiff base cryptand **1** and K, Rb, or Cs (or an excess of **1)** in THF at 233 K are green. Such solutions made with Li have a reddish color and those prepared with Na are orange. Figure 2a shows the spectrum of $\mathbf{1}^-$ reduced with 1 equiv of potassium. In addition to the visible bands at 415 and 654 nm, a distinguishing feature of the optical spectrum of $\mathbf{1}^-$ is a broad NIR band with a maximum at 1345 nm and a shoulder at 1180 nm. The position of one of the visible bands exhibits a bathochromic shift as the cation radius increases, with λ = 650, 654, 660, and 664 nm for Na^+, K^+, Rb^+, and Cs^+, respectively, at 233 K. The wavenumber of the peak is nearly proportional to the reciprocal of the cation radius. As shown in Figure 2b, the addition of the strong complexant

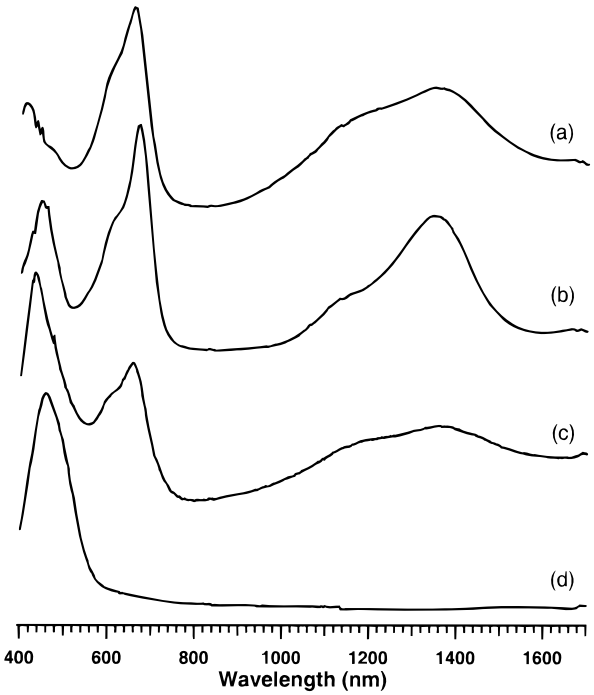

Figure 2. Optical spectra of **1** reduced with K in THF: (a) T = 233 K; (b) after the addition of 1 equiv of cryptand[2.2.2] to the solution in (a), T = 233 K; (c) $\mathbf{1}^{2-}$ prepared with 2 equiv of K, T = 243 K; (d) $\mathbf{1}^{3-}$ prepared with 3 equiv of K, T = 243 K.

for cations, cryptand[2.2.2] (C222)[28] results in a shift of the visible bands to 445 and 670 nm. The intensity of the 1345-nm band increases while that of the 1180-nm shoulder decreases. The spectrum in the presence of C222 is presumably that of the "cryptand-separated" radical anion pair, the analogue of a solvent-separated ion pair, and is referred to as the "free" anion spectrum. Similar changes in the spectrum of $\mathbf{1}^-$ were observed before and after complexation of the Na^+ cation with C222 in dimethyl ether. The absorption line shape of $Na^+\mathbf{1}^-$ in THF also changes dramatically and reversibly with temperature (shown in the Supporting Information). At 258 K, the optical spectrum is similar to that shown in Figure 2a with only the cation-dependent differences in the visible region (480- and 650-nm peaks), while at 188 K, the spectrum is nearly identical to that of the free monoanion shown in Figure 2b. For the larger

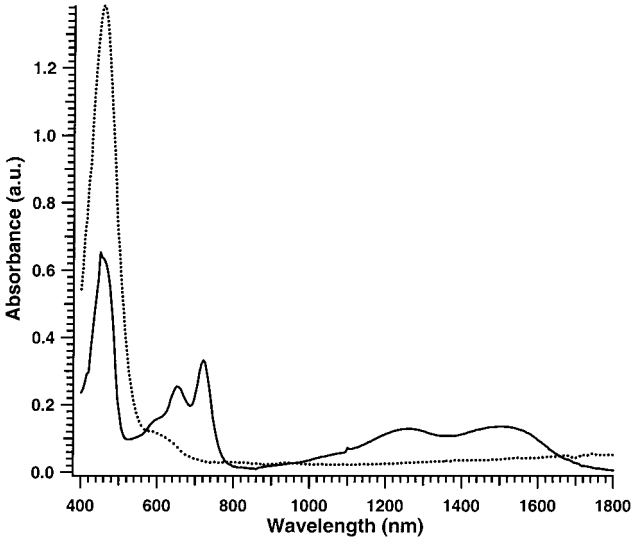

Figure 3. Optical spectra of K^+2^- before (broken line, $T = 240$ K) and after (solid line, $T = 228$ K) the addition of cryptand[2.2.2] to the THF solution.

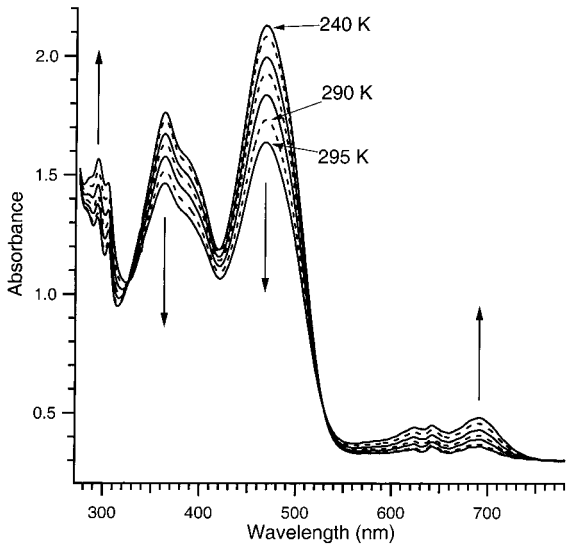

Figure 4. Optical spectra of a solution of the single strand **3** reduced with Rb in THF recorded at various temperatures (240, 250, 260, 270, 270, 290, and 295 K, alternating solid and dashed lines). Arrows indicate how the spectrum of 3^- changes with temperature.

cations, K^+, Rb^+, and Cs^+, the optical spectra do not vary significantly with temperature. As emphasized in the Discussion section, all of the results described above are consistent with the formation of contact ion pairs in THF for K, Rb, and Cs at all temperatures and Na at the higher temperatures. The addition of C222 breaks up the contact pairs as does increased solvation of Na^+ at lower temperatures (aided by the increase in the dielectric constant).

Solutions in THF with up to a 3:1 ratio of metal to complexant can also be obtained at low temperature (233 K). Upon reaction of **1** with alkali metal films, the green solution appears first, followed by gradual dissolution of the metal to yield a reddish solution 1−3 days later. The spectrum of such a solution, prepared with 3 equiv of K metal, is shown in Figure 2d. Note that the NIR bands have disappeared and the visible region is dominated by single absorption at 456 nm. The dianion could be prepared more readily by reduction with a stoichiometric amount of K metal. The optical spectrum of the resulting dianion (Figure 2c) has some of the same absorptions as the monoanion, but the NIR bands have decreased in intensity and a new feature at 425 nm has grown in.

The reduced forms of **1** are stable for long periods of time as long as the temperature is kept below 253 K. At room temperature, however, solutions of the mono-, di-, and trianion all evolve toward a reddish color in a matter of hours. The new spectra have a single absorption that appears between 460 and 510 nm, depending on the initial reduction state of **1** and the length of time the solution is kept at room temperature. Although the nature of these products of room-temperature decomposition is not known, all become colorless upon oxidation by air.

The reduction of the model compounds **2** and **3** by alkali metals in THF at 223−233 K results in the formation of reddish (Li, Na) to light orange (K, Rb, Cs) solutions. Figure 3 shows that the optical spectrum of **2** reduced with K is dominated by a single absorption band at 456 nm and a weak shoulder at 585 nm. As the solution is warmed from 223 K to room temperature, solutions of 2^- and 3^- take on a greenish tinge that is more pronounced with the larger cations Rb^+ and Cs^+. Figure 4 shows the variation in the optical spectrum with an increase in temperature for 3^- reduced with Rb metal in THF. These color changes are reversible upon temperature cycling as long as the solution is not kept at room temperature for prolonged periods. An orange solution of K^+2^- immediately turns bright green upon addition of C222 and shows new absorption bands at 450, 657, 720, 1260, and 1495 nm (Figure 3, solid line). The changes in the optical spectrum that occur upon the addition of C222 are not reversed by subsequent variations in temperature. The optical spectra of 3^- at 233 K both before (484 nm (s); 632, 690, (w); 1207, 1482 nm (vw)) and after the addition of C222 (415, 649, 709, 1259, 1506 nm (s)) are similar to those of 2^- and are included in the Supporting Information.

EPR and ENDOR. All of the colored solutions that represent the various reduction stages of the Schiff base cryptand**, 1,** are paramagnetic. However, when a solution of the mono-, di-, or trianion is kept at room temperature for about an hour, the resulting reddish solution is diamagnetic. Below 253 K the paramagnetism lasts indefinitely.

Hyperfine splitting (hfs) is observed from THF solutions of 1^- reduced by any of the alkali metals. For example, the spectrum of the Na^+1^- ion pair is shown in Figure 5a. Line-broadening effects tend to obscure the hfs at lower temperatures to yield featureless spectra with peak-to-peak line widths (ΔH_{pp}) of 0.84, 1.07, 1.24, and 1.5 mT for Na, K, Rb, and Cs, respectively. There is also a modest shift in the *g*-value as the size of the cation increases; $g = 2.002\,96$, 2.003 01, 2.003 11, and 2.003 36 for Na^+, K^+, Rb^+, and Cs^+, respectively. The addition of C222 to a THF solution of K^+1^- results in a featureless line (Figure 5b) with $\Delta H_{pp} = 0.84$ mT and $g = 2.002\,96$. The same spectral change is observed when methylamine is the primary solvent or is added by vacuum distillation to the THF solution.

Reduction of **1** in THF with 3 equiv (or a large excess) of K metal over a 2−3 day period at temperatures of 228−233 K results in a solution that has the EPR spectrum shown in Figure 5d. This spectrum can be correlated with the optical spectrum in Figure 2d since both spectra were obtained from the same preparation. Preparation of 1^{2-} by reaction with 2 equiv of metal results in an intermediate stage of reduction. The EPR spectrum of the dianion tended to vary somewhat from preparation to preparation. This is not surprising because a small amount of metal over or under the stoichiometric amount produces features that can be ascribed to the trianion or the monoanion, respectively. The hfs values for all of the reduced forms of **1** are metal-

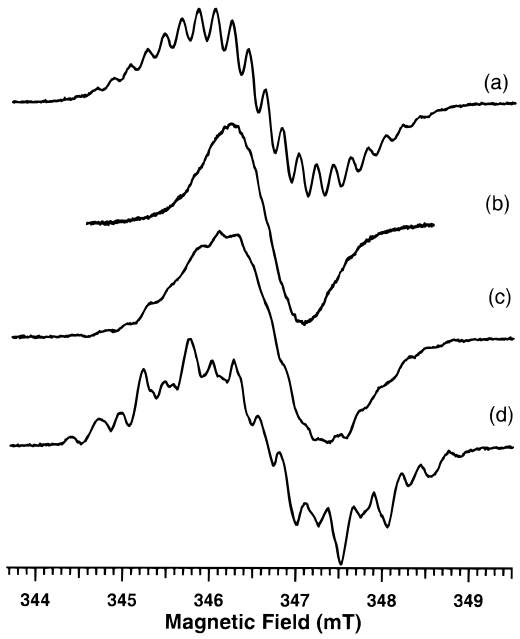

Figure 5. Solution EPR spectra of (a) $\mathbf{1}^-$ prepared with 1 equiv of Na in THF, $T = 253$ K; (b) $\mathbf{1}^-$ after the addition of cryptand[2.2.2]; (c) $\mathbf{1}^{2-}$ prepared with 2 equiv of K, $T = 249$ K; (d) $\mathbf{1}^{3-}$ prepared with 3 equiv of K, $T = 243$ K.

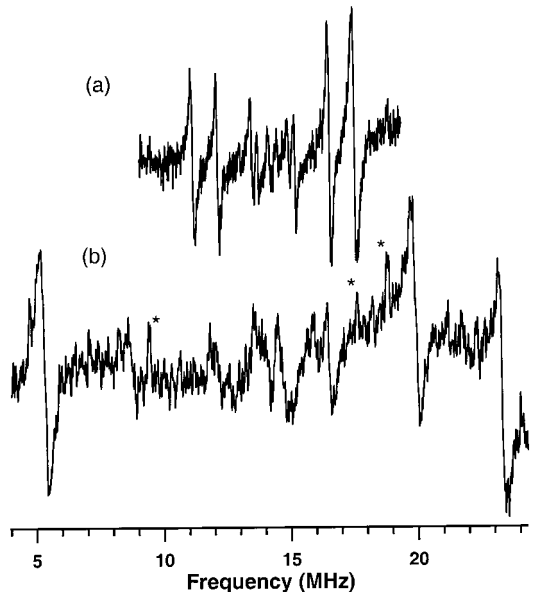

Figure 6. Solution ENDOR spectra of (a) the free monoanion, $\mathbf{1}^-$, in THF at 180 K, and (b) the contact ion pair $Cs^+\mathbf{1}^-$ in 2-MTHF at 233 K. The "*" denotes experimental artifacts in spectrum (b).

dependent. Figure 5c shows the EPR spectrum of the $(K^+)_2\mathbf{1}^{2-}$ ion triple for a sample in which the stoichiometry was controlled as closely as possible.

By setting the field at the center of the EPR spectrum of the "free" anion (with C222 present, Figure 5b), five sets of proton couplings were observed in the ENDOR spectrum, as shown in Figure 6a, and listed in Table 2. The relative signs of the four largest hfs couplings were determined by general triple-resonance experiments.[29] The same proton hfs constants were obtained from an ENDOR measurement of $\mathbf{1}^-$ reduced in THF with Na metal. At temperatures higher than 210 K the ENDOR effect was not observed. However, at temperatures below 210 K, an ENDOR spectrum appeared and attained sufficient resolution at 180 K to show that the spectrum was identical to that displayed in Figure 6a (the EPR line width was 0.84 mT peak-to-peak at 180 K). This result correlates well with the optical data for the same $Na^+\mathbf{1}^-$ adduct. Both sets of data indicate that contact ion pairs are dominant for the $Na^+\mathbf{1}^-$ adduct at higher temperatures, while below 210 K, partial dissociation into solvent-separated ion pairs and/or free ions occurs.

When the solvent was changed to 2-methyl-THF and $\mathbf{1}^-$ was prepared by reduction with Cs, the ENDOR spectrum shown in Figure 6b was observed. Five sets of hfs can be measured directly and a sixth pair probably overlaps the smallest hfs. A similar spectrum was also observed from the $Na^+\mathbf{1}^-$ ion pair in 2-MTHF solution at 233 K, but the resolution of the two or three smallest splittings was poor. The hfs constants of $\mathbf{1}^-$ in its ion-paired form with the Cs^+ and Na^+ cations are given in Table 2. General triple-resonance experiments were unsuccessful for these samples, so the relative signs of the hfs constants could not be determined. The ENDOR effect diminished rapidly below 223 K, contrary to typical ENDOR conditions for maximum signal enhancement.[29]

Resonances attributable to the ^{133}Cs or ^{23}Na cations were not observed in ENDOR experiments. Proton ENDOR spectra were not obtained for the di- and trianions despite numerous attempts.

The color changes observed for the model compounds $\mathbf{2}^-$ and $\mathbf{3}^-$ during variations in temperature can be correlated with the EPR signal intensity. At 233 K, THF solutions of $\mathbf{2}^-$ and $\mathbf{3}^-$ are very weakly paramagnetic and by 193 K are essentially diamagnetic. As the temperature is increased, the paramagnetism of the solutions also increases so that near room temperature an EPR signal can be observed. (With 2-MTHF as the solvent, no EPR signal attributable to $\mathbf{2}^-$ can be detected at any temperature until C222 is added to the solution.) The correlation between the EPR signal and the color indicates that the greenish tinge observed at higher temperatures is that of a paramagnetic species, while the orange color (optical spectrum, Figure 3, broken line) is assigned to a diamagnetic species. If the temperature is held at 293 K for more than 1 h, the solution becomes diamagnetic and the temperature effects are irreversible, indicating that decomposition has occurred. An intense EPR spectrum with extensive hyperfine splitting and a very narrow line width ($\Delta H_{pp} \sim 0.01$ mT) was observed when C222 was added to a fresh solution at 233 K (Figure 7a). The identical spectrum was produced when the reduction was carried out in methylamine. The variation of the intensity of this spectrum with temperature is opposite to that obtained without C222 or methylamine. We conclude that either C222 or methylamine with $\mathbf{2}^-$ yields the strongly paramagnetic species that is responsible for the solid line optical spectrum shown in Figure 3.

The THF solutions of $\mathbf{2}^-$ and $\mathbf{3}^-$ with C222 present were suitable for ENDOR experiments over a broad temperature range (170−220 K). With the static field placed at a line near the center of the EPR spectrum, the ENDOR spectrum of the free ion $\mathbf{2}^-$ was obtained (Figure 7c). Five sets of proton hfs constants can be determined from the ENDOR spectrum and are listed in Table 2. The protons were assigned with the help of general triple ENDOR to determine the relative sign of the hfs as well as with the help of ab initio calculations. The calculated hfs constants and absolute signs of the hfs for compound $\mathbf{2}^-$ (assuming planarity) with the BLYP/6-31g*// BLYP/6−31g* calculation[30−32] are also listed in Table 2 for comparison. The hfs constant of the 2 equiv Schiff base nitrogen atoms, a_N, was determined by adjusting its value until the simulated EPR spectrum of $\mathbf{2}^-$ (Figure 7b) matched the experimentally observed one. The hfs constants of $\mathbf{3}^-$ determined

TABLE 2: Proton Hyperfine Splittings of 1^-, 2^-, and 3^- Determined from ENDOR Experiments, Simulation of the EPR Spectra, and Density Functional Theory

sample and conditions	hyperfine splitting in mT and number of equivalent atoms in parentheses						
			Experiment				
1^-/K/THF/C222; 180 K	−0.226 (6H)	+0.157(12H)	−0.062 (6H)	+0.042 (3H)	<0.01 (3H)	0.012 (12H)	0.076[a] (6N)
1^-/Cs/2-MTHF; 233 K	0.642 (2H)	0.399 (4H)	0.155 (2H)	0.118 (1H)	0.020 (1H)	0.040 (4H)	0.227[a] (2N)
1^-/Na/2-MTHF; 233 K	0.624 (2H)	0.302 (4H)	0.133 (2H)				
2^-/K/THF/C222; 170 K	−0.703 (2H)	+0.306 (6H)	−0.184 (2H)	+0.131 (1H)	0.009 (1H)		0.234[a] (2N)
3^-/K/THF/C222; 200 K	−0.703 (2H)	+0.056 (2H)	−0.184 (2H)	+0.132 (1H)	0.014 (1H)	+0.014(12H)	0.226[a] (2N)
			Theory				
2^- BLYP/6-31g*[b]	−0.685 (2H)		−0.235 (2H)	+0.131 (1H)	+0.032 (1H)		+0.244 (2N)

[a] Determined by simulation of the EPR spectrum. [b] Density functional theory calculation at the BLYP/6-31g*//BLYP/6−31g* level of theory.

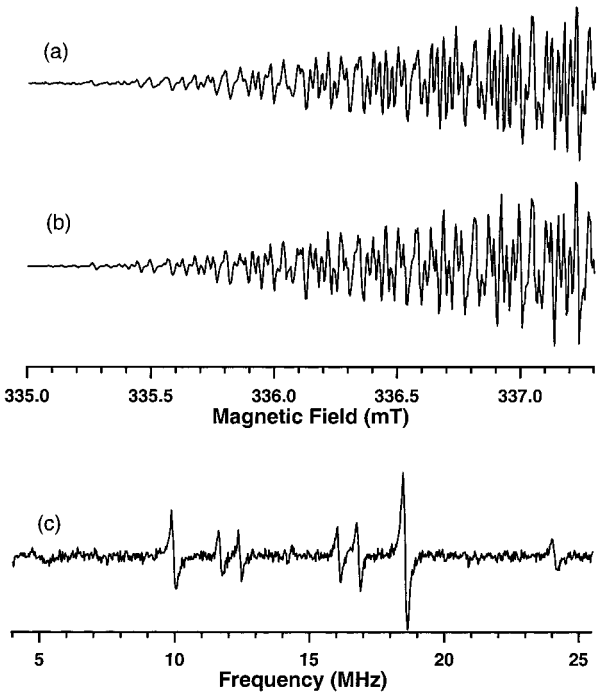

Figure 7. (a) One-half of the solution EPR spectrum of the free monoanion, 2^-, and (b) the simulated spectrum. The full spectra are reproduced in the Supporting Information. (c) Solution ENDOR spectrum of the free anion, 2^-.

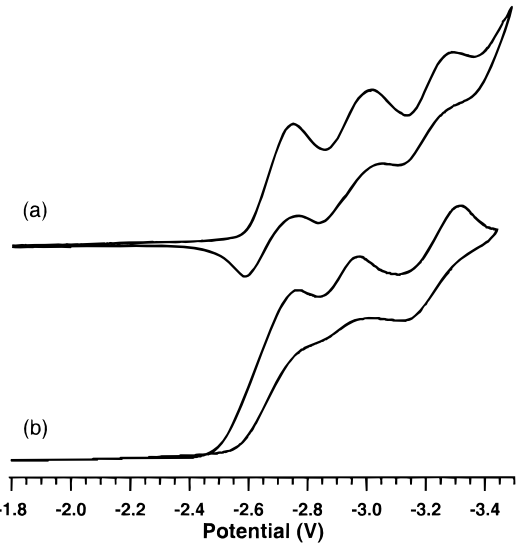

Figure 8. Cyclic voltammogram of (a) **1** showing a near-reversible three electron reduction and (b) **3** showing an irreversible multielectron reduction. Both experiments were carried out in THF at room temperature with a sweep rate of 0.1 V s^{-1}.

by double- and triple-resonance experiments are also listed in Table 2. The observed and simulated EPR spectra as well as the ENDOR spectrum of model compound 3^- were obtained with equal resolution and are included in the Supporting Information.

Electrochemistry. Cyclic voltammetry confirmed that the Schiff base cryptand could be multiply reduced. Three reduction waves at −2.66, −2.98, and −3.26 V with respect to ferrocene/ferrocinium (Figure 8a) are clearly visible, indicating that **1** is capable of accepting at least three electrons with partial reversibility. The electrochemistry of the single-strand molecules is less clear. Under the conditions of the electrochemistry experiment, the reduction of **2** and **3** is irreversible. Figure 8b shows that **3** does not have a distinct one-electron reduction potential. Instead, two or three waves are observed during reduction while the features in the subsequent oxidation step are faint.

Discussion

The structure of cryptand **1** consists of three strands that are linked to the tertiary amine nitrogen atoms via saturated carbon bridges. The π-system of each strand is thus somewhat isolated from the others in comparison to more fully conjugated planar aromatics. The crystal structure shows that the strands are well separated from each other so that the overlap between π-systems is poor because of the spatial orientation of each strand. Although the structure of 1^- may be somewhat different in solution, these general characteristics seem to be responsible for the various features of the optical and magnetic resonance spectra.

For 1^- formed by reduction in THF with any of the alkali metals (except lithium), the optical and EPR spectra at higher temperatures can confidently be ascribed to the contact ion pair. This is evident because the addition of C222 or methylamine causes an immediate and irreversible change in the spectra and removes any temperature-dependent spectral variations. Further evidence for contact ion pairs comes from the cation-dependent bathochromic shift in one of the visible absorption bands. The solution EPR studies show a shift in the *g*-value with varying alkali metal cation sizes, additional evidence for contact ion pairs. Na^+ forms a contact ion pair at higher temperatures, but the equilibrium shifts toward solvent-separated or free ions at lower temperatures. The larger cations still form contact ion pairs that increase in stability from K^+ to Cs^+, as shown by their residual EPR line widths at low temperatures, which remain broad compared to that of the free ion. These observations are consistent with documented trends of ion pair equilibria for a wide variety of reduced species.[1,2]

It is informative to compare the optical spectrum of the model single-strand "free" ions 2^- (Figure 3) and 3^- (Figure 4) with the spectra of the contact ion pair and free ion forms of the

Schiff base cryptand $\mathbf{1}^-$ (Figures 2a and 2b). Although the NIR region of $\mathbf{2}^-$ is somewhat red-shifted in comparison to $\mathbf{1}^-$ and the bands of $\mathbf{1}^-$ are broader, the optical spectrum of $\mathbf{2}^-$ with C222 is generally similar to that of $\mathbf{1}^-$. The similarity between the optical spectra of $\mathbf{2}^-$, $\mathbf{3}^-$, and $\mathbf{1}^-$ indicates that the optical transitions observed for $\mathbf{1}^-$ occur from a *single strand* of the cryptand. In other words, on the optical time scale, the unpaired electron on $\mathbf{1}^-$ is localized to one strand of the cryptand in both the free ion and the contact ion pair. This means that the NIR bands of $\mathbf{1}^-$ are not the result of intramolecular charge transfer between the strands. Intermolecular charge transfer that might take place between charged and neutral species is also unlikely because of the controlled stoichiometric reduction of the organic substrates and the dilute solutions used.

As the cyclic voltammogram shows, **1** can accept three electrons with partial reversibility. The addition of a second electron to $\mathbf{1}^-$ results in only modest changes of the optical spectrum. Absorptions similar to those of the monoanion are observed in addition to a new absorption at 436 nm. This suggests that, even with two electrons, the optical spectrum of the dianion can be accounted for largely in terms of transitions within single strands. However, a remarkable change in the optical spectrum occurs with the addition of a third electron to **1**. The NIR absorptions from single strands disappear and only one intense band remains at 456 nm. If the 456-nm band is characteristic of the trianion, then this observation implies that the three unpaired electrons interact through bond or through space to shift the molecular orbital energies. The possibility that the 456-nm absorption is due to an intra- or intermolecular dimer is unlikely because at least one reduced strand would remain after dimerization. This would leave absorptions similar to those of the monoanion and dianion.

The following experiments were performed to confirm that the formation of the trianion is reversible. When 2 equiv (or an excess) of the neutral Schiff base cryptand were dissolved and added to a THF solution of $(K^+)_3\mathbf{1}^{3-}$, the interfacial region between the two solutions changed to the characteristic green color of the monoanion reduced with potassium. After mixing of the neutral and anionic solutions was complete, the solution was reddish-brown and the optical spectrum displayed absorptions characteristic of the monoanion in addition to a band at ~456 nm, similar to that of the trianion. The EPR spectrum, however, consisted entirely of the monoanion without a trace of the trianion spectrum. Clearly, conversion to the monoanion occurred, but the incomplete conversion of the optical spectrum needs explanation. Diamagnetic decomposition products have a broad absorption band in this region and may be responsible for the apparent incomplete conversion of the trianion to the monoanion. Similar results were obtained with a solution of $(K^+)_3\mathbf{1}^{3-}$ in $MeNH_2$ except that the conversion of the optical spectrum to that of the monoanion was less complete and slow, probably because of the very limited solubility of the cryptand **1** in methylamine.

It is known that the EPR spectra of quartet ($S = {}^3/_2$) states sometimes show a "third-field" or $\Delta m_S = 3$ transition in addition to the half-field or $\Delta m_S = 2$ transition characteristic of spin states in which $S \geq 1$.[33] Therefore, a frozen THF solution of $(K^+)_3\mathbf{1}^{3-}$ was studied by EPR between 4 and 100 K. At 21 K, the intense EPR spectrum had two resonances ~12.0 mT apart that could be ascribed to the outermost parallel $\Delta m_S = \pm 1$ transitions of a quartet ($S = {}^3/_2$) state. While a distinct but weak half-field transition ($\Delta m_S = 2$) was observed, the confirming $\Delta m_s = 3$ transition was absent. This absence is not unexpected because the relative intensities of the three transitions vary as

SCHEME 1

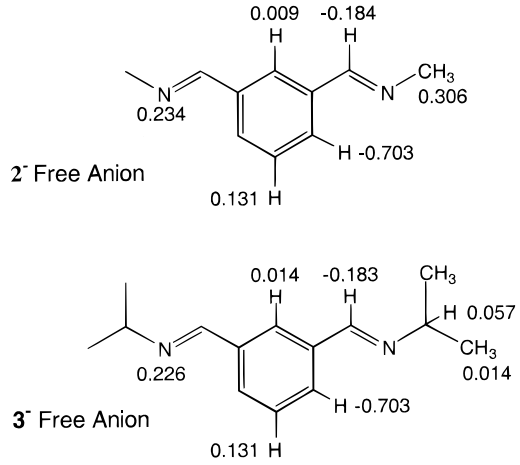

$1:(D/H)^2:(D/H)^4$.[33] With an effective D-value of only 3.0 mT, the $\Delta m_S = 3$ transition would be completely lost in the noise.

Because coupling between strands of $\mathbf{1}^-$ is expected to be weak, the distribution of the unpaired electron spin in $\mathbf{2}^-$ can be used to interpret the solution EPR spectra of $\mathbf{1}^-$. The multitude of overlapping lines in the EPR spectrum of $\mathbf{2}^-$ can be completely understood by using just five pairs of resonances from the proton ENDOR spectrum. The close similarity between the simulated and experimental spectrum (Figure 7) shows that the hfs constant of nitrogen was accurately determined and that the protons were assigned correctly. As shown in Table 2, density functional theory did a credible job of predicting the magnitude of the hfs for both protons and nitrogens and enabled the determination of the absolute signs of the hfs, information that proved critical for assigning couplings of similar magnitude to the correct protons. The hyperfine splittings of radical anion $\mathbf{3}^-$ are virtually identical to those of $\mathbf{2}^-$ except for the isopropyl group. On the basis of triple-resonance experiments, both sets of protons on the isopropyl group have the same absolute sign. The assignment of the hfs for both model compounds is illustrated in Scheme 1.

Although the EPR spectrum of the *free anion* of $\mathbf{1}^-$ is essentially featureless, the ENDOR spectrum reveals five sets of proton hfs constants. It is significant that the three largest proton hfs constants and the nitrogen hfs in the conjugated region are approximately one-third those of the corresponding nuclei of $\mathbf{2}^-$ and that the relative signs of the proton hfs are also the same (Table 2 and Schemes 1 and 2). The sixth proton hfs in this region is either too weak to observe or overlaps another line in the ENDOR spectrum of $\mathbf{1}^-$. The hfs constant of the 6 equivalent nitrogen atoms (a_N) was determined by simulating the EPR spectrum of the free anion. This procedure used the experimental proton hfs couplings and adjusted a_N until the overall line width of the EPR spectrum was matched. The 3-fold decrease of the three proton hfs constants and that of nitrogen provides strong evidence that the unpaired electron in the free ion $\mathbf{1}^-$ is delocalized over the three strands on the NMR time scale (10^{-7} s).

A very different ENDOR spectrum of $\mathbf{1}^-$ is obtained (Figure 6b) when the experimental conditions are adjusted to favor contact ion pairs. The magnitudes of the hfs constants of the $Cs^+\mathbf{1}^-$ adduct are very similar to those of $\mathbf{2}^-$, although the signs could not be determined. On the basis of their magnitudes, the protons were assigned as shown in Scheme 2 for the contact ion pair. The solution EPR spectra of the $Cs^+\mathbf{1}^-$ adduct acquired in the temperature range 213−253 K were simulated with the hfs constants shown in Scheme 2, together with adjustable

SCHEME 2

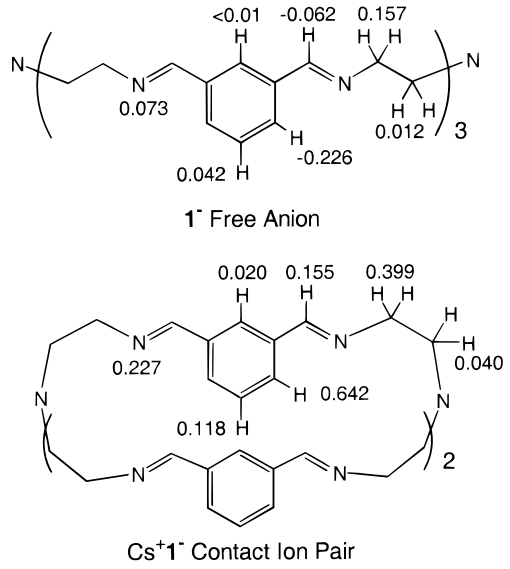

parameters to account for the hfs due to the Schiff base nitrogens (a_N) and hfs from a single Cs^+ nucleus (a_{Cs}^+). Addition of the parameter a_{Cs}^+ is not unreasonable in view of the experimental conditions, even though ^{133}Cs-ENDOR was not observed experimentally. The simulations were carried out with the nonlinear least-squares fitting program, KINFIT,[34] that adjusted the unknown parameters, such as the line width, a_{Cs}^+, a_N, and scale factor, until the sum of the squares of the residuals was a minimum. An excellent fit was obtained for all temperatures and an example is shown in Figure 9. It was found that a_N did not vary significantly ($a_N = 0.2265 \pm 0.0015$ mT) over the temperature range investigated, while a_{Cs}^+ increased as the temperature was lowered, with $a_{Cs}^+ = 0.229$, 0.232, 0.237, 0.242, and 0.251 mT at $T = 253$, 243, 233, 223, and 213 K, respectively. The temperature effect on a_{Cs}^+ is an excellent indication that the sign of the Cs^+ hfs constant is negative.[35,36] The unpaired electron in the $Cs^+\mathbf{1}^-$ adduct is therefore *localized* to one strand of the Schiff base cryptand on the NMR time scale.

Clearly, the rate of interstrand electron transfer is governed by the conditions that stabilize the cation. Because cation migration and electron transfer must proceed together, there must be a concomitant rearrangement of the solvent shell and ion pair structure. The height of the energy barrier for this process depends on the prevailing experimental conditions. Delocalization requires a rate of electron transfer that is on the order of the hyperfine splitting constant or larger. For example, when the cation is stabilized by C222, methylamine, or low temperatures (for a small cation such as Na^+) in THF, the rate of electron transfer in $\mathbf{1}^-$ is greater than 4×10^7 s^{-1}. (This estimate is based on the quantity $2\pi(^1/_2\Delta a)$ in which $\Delta a = a_{CIP} - a_{FI}$ is the difference between the largest proton hfs constants for the contact ion pair and free ion from lines 2 and 1, respectively, in Table 2.) The result is an isotropic EPR line in which the electron is *apparently* delocalized over the three strands of **1**. On the other hand, large cations such as Cs^+, a solvent with low polarity (2-MTHF), and high temperatures favor contact ion pairs, in which the rate of intramolecular electron transfer is less than 4×10^7 s^{-1}. Under the latter conditions, the electron is localized to a single strand of the cryptand on the NMR time scale. Similar observations concerning the rate of intramolecular electron transfer were reported for other radical anions with saturated bridges between aromatic groups.[37−39] A different

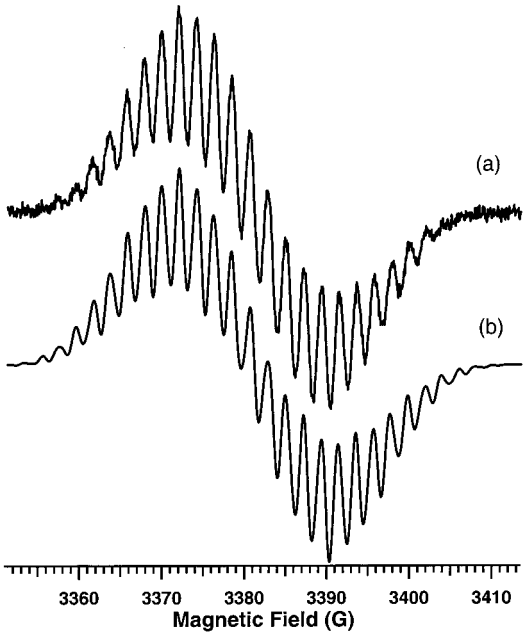

Figure 9. Comparison of the (a) experimental and (b) simulated EPR spectrum of the $Cs^+\mathbf{1}^-$ adduct in 2-MTHF at 253 K.

situation exists for the completely reduced $\mathbf{1}^{3-}$. Because each strand contains an "excess" electron and its counterion, the rate of electron transfer does not determine the extent of hyperfine splitting. In this case, it is expected that the magnitude of the hfs would be very close to that of $\mathbf{2}^-$ and $\mathbf{3}^-$. The EPR spectra suggest that this is true, but it was not possible to simulate the spectra of $\mathbf{1}^{3-}$ salts quantitatively.

The solution chemistry of the model compounds $\mathbf{2}^-$ and $\mathbf{3}^-$ deserves further comment. The reversible changes in the optical and EPR spectra that occur with temperature suggest that the monoanion is in equilibrium with a diamagnetic dimer. Reversibility of this dimerization process is dramatically shown by the complete and rapid reversal upon addition of C222. The tendency to dimerize is rather strong, so that even with a large excess of ligand (6:1, ligand to metal) the spectroscopic observations follow the same trends with temperature as stoichiometric 1:1 preparations. The dimer forms quickly and preferentially in THF so that a distinct monoreduced species is not present in solution at high concentrations, even at room temperature. Other factors besides temperature and solvent influence the monomer−dimer equilibrium. The largest cation, Cs^+ (and Rb^+ to some extent), shifts the equilibrium toward the monomer to a greater extent than do the cations with smaller ionic radii. In addition, the model anion $\mathbf{3}^-$, which has the bulkier isopropyl substituent, tended to have a higher concentration of monomer at a given temperature with the same metal than that of $\mathbf{2}^-$. These qualitative observations are based on comparisons of solution EPR spectra. However, the EPR signal intensity is still much less than that of the free ion for both **2** and **3**. Therefore, the optical spectrum shown in Figure 3 (broken line) must be due to the dimer of $\mathbf{2}^-$.

Herein lies one of the difficulties in performing the electroreduction of **2** and **3**. The monomer−dimer equilibrium is sensitive to cation size, temperature, and solvent. It is also likely that the necessary introduction of a large excess of supporting electrolyte in the electrochemistry experiments may influence the equilibrium. Therefore, the lack of distinct symmetrical reduction waves is probably due to reduction of the model compound to the monoanion followed by rapid dimer formation and subsequent reduction of the dimer. It is noteworthy that

SCHEME 3

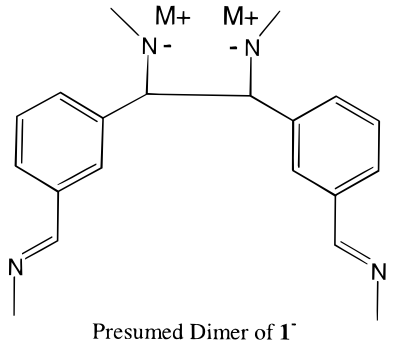

Presumed Dimer of $\mathbf{1}^{\cdot}$

the dianion of **2** could not be prepared by alkali metal reduction, even in a solvent that promotes metal dissolution such as methylamine. It is therefore unlikely that $\mathbf{2}^{2-}$ or $\mathbf{3}^{2-}$ contribute to the cyclic voltammogram.

Contact ion pairs are necessary for dimer formation because polar, coordinating solvents, and complexants that stabilize the cation lead to the free monoanion. While it is not possible to rule out a stacked structure formed by $\pi-\pi$ interactions, the lack of long wavelength transitions, especially in the NIR, suggests that the dimer is in fact a closed shell species.[40−42] A possible structure for the dimers of $\mathbf{2}^-$ and $\mathbf{3}^-$ analogous to the pinacolate dimer formed by two ketyl radicals is illustrated in Scheme 3. Contrary to the diamagnetic pinacolate dimer of sodium flourenone that is formed only in minute quantities in ethereal solvents,[43] dimers of $\mathbf{2}^-$ and $\mathbf{3}^-$ predominate in THF. In fact, a shift to diamagnetic solutions of $\mathbf{2}^-$ at all temperatures occurs when the solvent is changed to 2-MTHF. The lack of long-wavelength absorptions in the optical spectra and the aforementioned changes in the monomer−dimer equilibrium with cation size and nitrogen substituent support carbon−carbon bond formation as the most likely structure for the dimer because steric interactions would be accentuated in the restricted quarters of the pinacolate-like structure. There is no evidence for dimer formation with the Schiff base cryptand, $\mathbf{1}^-$.

When samples of $\mathbf{2}^-$ and $\mathbf{3}^-$ were frozen in liquid nitrogen and left uncovered on the bench for some time, the samples took on a greenish color similar to the free monoanion in solution. A simple experiment showed that ambient light in the laboratory caused the changes in color. Saturation of the greenish color took place after about an hour at 77 K. The "photolyzed" sample was quickly placed in the EPR cavity at 4 K without the EPR tube being warmed. A robust triplet ($S = 1$) signal was observed and identified by its characteristic $\Delta m_S = \pm 1$ and half-field transitions. The magnitude of the zero field splitting parameters depends on the metal cation and a full discussion of the solid-state phenomena including triplet-state ENDOR will be reported separately. This may be the first reported instance of conversion from a diamagnetic radical anion dimer to a paramagnetic triplet by photolysis in the solid state.

Conclusions

The solution chemistry of the Schiff base cryptand monoanion is governed by ion pair equilibria. Optical, EPR, and ENDOR spectra were used to determine the effect of temperature, solvent, and cation radius on the extent of contact ion pair, solvent-separated ion pair, and free ion formation. Ion pair formation affects the rate of interstrand electron transfer and, thus, the appearance of the EPR spectra. Only limits of the electron-transfer rates (4×10^7 s^{-1}) can be obtained from the ^1H hyperfine frequencies. Contact pair formation yields slower transfer rates while the rate is greater for solvent- or complexant-separated ion pairs. With the possible exception of the trianion, all interstrand electron transfers are slow on the *optical* time scale.

The macrobicyclic Schiff base cryptand, while an excellent electron acceptor, is a poor complexant for the alkali metals Na, K, Rb, and Cs in THF. The best candidate for complexation is the lithium cation, which has an affinity for nitrogen and a tetrahedral coordination sphere. The structures of Cu(I) salts[44,45] show that cryptands of this type may accommodate two cations bound in the pseudo-tetrahedral pockets formed by three Schiff base groups and the capping nitrogen atoms. Accordingly, we are attempting to grow crystals by reducing **1** with 2 equiv of lithium under a variety of conditions. Modification of the original complexant design is also underway to produce cryptands with a higher reduction potential and better ability for cation complexation.

Acknowledgment. This research was supported in part by the NSF Grant DMR-96-10335 and AFOSR Grant F49620-92-J-0523 and by the Center for Fundamental Materials Research at Michigan State University. A scholarship from the Region Nord-Pas de Calais (France) for F.D. and the support of FEDER are gratefully acknowledged.

Supporting Information Available: Optical spectra of $Na^+\mathbf{1}^-$ and $K^+\mathbf{3}^-$ in THF; observed and calculated EPR spectra of $\mathbf{2}^-$ and $\mathbf{3}^-$ and ENDOR spectrum of $\mathbf{3}^-$; tables of crystal data, atomic coordinates, bond lengths and angles, and general thermal parameters for $K^+\mathbf{1}^-(MeNH_2)_6$. [(PDF) as well as X-ray crystallographic files (CIF)]. This material is available free of charge via the Internet at http://pubs.acs.org

References and Notes

(1) Szwarc, M. *Ions and Ion Pairs in Organic Reactions*; Wiley-Interscience: New York, 1972; Vol. 1, pp 1−399.
(2) Szwarc, M. *Ions and Ion Pairs in Organic Reactions*; Wiley-Interscience: New York, 1974; Vol. 2, pp 1−566.
(3) Thompson, J. C. *Electrons in Liquid Ammonia*; Oxford University Press: Oxford, 1976; pp 1−297.
(4) Dye, J. L. *Prog. Inorg. Chem.* **1984**, *32*, 327−441.
(5) Bock, H.; Herrmann, H. F.; Fenske, D.; Goesmann, H. *Angew. Chem., Int. Ed. Engl.* **1988**, *27*, 1067−1069.
(6) Bock, H.; Nather, C.; Ruppert, K.; Havlas, Z. *J. Am. Chem. Soc.* **1992**, *114*, 6907−6908.
(7) Bock, H.; Arad, C.; Nather, C.; Havlas, Z. *J. Chem. Soc., Chem. Commun.* **1995**, 2393−2394.
(8) Bock, H.; Ansari, M.; Nagel, N.; Claridge, R. F. C. *J. Organomet. Chem.* **1995**, *501*, 53−60.
(9) Bock, H.; John, A.; Nather, C.; Havlas, Z. *J. Am. Chem. Soc.* **1995**, *117*, 9367−9368.
(10) Bock, H.; Nather, C.; Havlas, Z. *J. Am. Chem. Soc.* **1995**, *117*, 3869−3870.
(11) Hou, Z. M.; Fujita, A.; Yamazaki, H.; Wakatsuki, Y. *J. Am. Chem. Soc.* **1996**, *118*, 2503−2504.
(12) Bock, H.; Havlas, Z.; Hess, D.; Nather, C. *Angew. Chem., Int. Ed. Engl.* **1998**, *37*, 502−504.
(13) Bock, H.; Lehn, J. M.; Pauls, J.; Holl, S.; Krenzel, V. *Angew. Chem., Int. Ed.* **1999**, *38*, 952−955.
(14) Dye, J. L. *Inorg. Chem.* **1997**, *36*, 3816−3826.
(15) Echegoyen, L.; Decian, A.; Fischer, J.; Lehn, J. M. *Angew. Chem., Int. Ed. Engl.* **1991**, *30*, 838−840.
(16) Echegoyen, L.; Xie, Q. S.; Perezcordero, E. *Pure Appl. Chem.* **1993**, *65*, 441−446.
(17) Echegoyen, L.; Perezcordero, E.; Devains, J. B. R.; Roth, C.; Lehn, J. M. *Inorg. Chem.* **1993**, *32*, 572−577.
(18) Perezcordero, E.; Buigas, R.; Brady, N.; Echegoyen, L.; Arana, C.; Lehn, J. M. *Helv. Chim. Acta* **1994**, *77*, 1222−1228.
(19) Wagner, M. J.; Dye, J. L.; Pérez-Cordero, E.; Buigas, R.; Echegoyen, L. *J. Am. Chem. Soc.* **1995**, *117*, 1318−1323.
(20) Perezcordero, E. E.; Campana, C.; Echegoyen, L. *Angew. Chem., Int. Ed. Engl.* **1997**, *36*, 137−140.

(21) Lappas, A.; Prassides, K.; Vavekis, K.; Arcon, D.; Blinc, R.; Cevc, P.; Amato, A.; Feyerherm, R.; Gygax, F. N.; Schenck, A. *Science* **1995**, *267*, 1799−1802.
(22) Haddon, R. C.; Hebard, A. F.; Rosseinsky, M. J.; Murphy, D. W.; Duclos, S. J.; Lyons, K. B.; Miller, B.; Rosamilia, J. M.; Fleming, R. M.; Kortan, A. R.; Glarum, S. H.; Makhija, A. V.; Muller, A. J.; Eick, R. H.; Zahurak, S. M.; Tycko, R.; Dabbagh, G.; Thiel, F. A. *Nature* **1991**, *350*, 320−322.
(23) Hebard, A. F.; Rosseinsky, M. J.; Haddon, R. C.; Murphy, D. W.; Glarum, S. H.; Palstra, T. T. M.; Ramirez, A. P.; Kortan, A. R. *Nature* **1991**, *350*, 600−601.
(24) Demol, F.; Sauvage, F. X.; Devos, A.; De Backer, M. G. *Synth. Met.* **1999**, *99*, 155−162.
(25) McDowell, D.; Nelson, J. *Tetrahedron Lett.* **1988**, *29*, 385−386.
(26) McKee, V.; Robinson, W. T.; McDowell, D.; Nelson, J. *Tetrahedron Lett.* **1989**, *30*, 7453−7456.
(27) Dye, J. L. *J. Phys. Chem.* **1984**, *88*, 3842−3846.
(28) IUPAC name: C222 = 4,13,16,21,24-hexaoxa-1,10-diazabicyclo-[8.8.8]hexacosane.
(29) Kurreck, H.; Kirste, B.; Lubitz, W. *Electron Double Resonance Spectroscopy of Radicals in Solution*; VCH: Weinheim, Germany, 1988; pp 1−374.
(30) Lee, C. T.; Yang, W. T.; Parr, R. G. *Phys. Rev. B* **1988**, *37*, 785−789.
(31) Becke, A. D. *Phys. Rev. A* **1988**, *38*, 3098−3100.
(32) Frisch, M. J.; Trucks, G. W.; Head-Gorden, M.; Gill, P. M. W.; Wong, M. W.; Foresman, J. B.; Johnson, B. G.; Schlegel, H. B.; Robb, M. A.; Replogle, E. S.; Gomperts, R.; Andres, J. L.; Rahavachari, K.; Binkley, J. S.; Gonzalez, C.; Martin, R. L.; Fox, D. J.; Defrees, D. J.; Baker, J.; Stewart, J. J. P.; Pople, J. A. *Gaussian 92*; Gaussian, Inc.: Pittsburgh, PA, 1992.
(33) Brickmann, J.; Kothe, G. *J. Chem. Phys.* **1973**, *59*, 2807−2814.
(34) Dye, J. L.; Nicely, V. A. *J. Chem. Educ.* **1971**, *48*, 443−448.
(35) De Boer, E. *Recueil Trav. Chim. Pays-Bas* **1965**, *84*, 609−625.
(36) Sommerdijk, J. L.; DeBoer, E. In *Ions and Ion Pairs in Organic Reactions*; Szwarc, M., Ed.; Wiley-Interscience: New York, 1972; Vol. 1, pp 340−351.
(37) Fuderer, P.; Gerson, F.; Heinzer, J.; Mazur, S.; Ohya-Nishiguchi, H.; Schroeder, A. H. *J. Am. Chem. Soc.* **1979**, *101*, 2275−2281.
(38) Harriman, J. E.; Maki, A. H. *J. Chem. Phys.* **1963**, *39*, 778−786.
(39) Shimada, K.; Szwarc, M. *J. Am. Chem. Soc.* **1975**, *97*, 3313−3321.
(40) Hausser, K. H.; Murrell, J. N. *J. Chem. Phys.* **1957**, *27*, 500−504.
(41) Boyd, R. H.; Phillips, W. D. *J. Chem. Phys.* **1965**, *43*, 2927−2929.
(42) Staples, T. L.; Szwarc, M. *J. Am. Chem. Soc.* **1970**, *92*, 5022−5027.
(43) Hirota, N.; Weissman, S. I. *J. Am. Chem. Soc.* **1964**, *86*, 2538−2545.
(44) Unpublished results, this laboratory.
(45) Jazwinsky, J.; Lehn, J.-M.; Lilienbaum, D.; Ziessel, R.; Guilheim, J.; Pascard, J. *J. Chem. Soc., Chem. Commun.* **1987**, 1691−1694.